LETTERS

Slip-stick and the evolution of frictional strength

Oded Ben-David[1], Shmuel M. Rubinstein[1]† & Jay Fineberg[1]

The evolution of frictional strength has great fundamental and practical importance. Applications range from earthquake dynamics[1–4] to hard-drive read/write cycles[5]. Frictional strength is governed by the resistance to shear of the large ensemble of discrete contacts that forms the interface that separates two sliding bodies. An interface's overall strength is determined by both the real contact area and the contacts' shear strength[6,7]. Whereas the average motion of large, slowly sliding bodies is well-described by empirical friction laws[3,8–10], interface strength is a dynamic entity that is inherently related to both fast processes such as detachment/re-attachment[11–14] and the slow process of contact area rejuvenation[6,7,13,15,16]. Here we show how frictional strength evolves from extremely short to long timescales, by continuous measurements of the concurrent local evolution of the real contact area and the corresponding interface motion (slip) from the first microseconds when contact detachment occurs to large (100-second) timescales. We identify four distinct and inter-related phases of evolution. First, all of the local contact area reduction occurs within a few microseconds, on the passage of a crack-like front. This is followed by the onset of rapid slip over a characteristic time, the value of which suggests a fracture-induced reduction of contact strength before any slip occurs. This rapid slip phase culminates with a sharp transition to slip at velocities an order of magnitude slower. At slip arrest, 'ageing' immediately commences as contact area increases on a characteristic timescale determined by the system's local memory of its effective contact time before slip arrest. We show how the singular logarithmic behaviour generally associated with ageing is cut off at short times[16]. These results provide a comprehensive picture of how frictional strength evolves from the short times and rapid slip velocities at the onset of motion to ageing at the long times following slip arrest.

Although frictional motion is often conceptually viewed as the motion of two rigid bodies in perfect contact at a planar interface, in fact, the applied normal load F_N is supported by an ensemble of micro-contacts that comprise only a small fraction of the apparent contact area. The real contact area A of these micro-contacts determines the interface strength[6,7]. The interface's properties differ entirely from those of the surrounding elastic material[17], because it bears local pressures that approach the material yield strength. How these contacts detach and re-attach is central to understanding frictional motion.

Frictional slip[18,19] initiates rapidly, through the fracture of contacts. A number of different fracture mechanisms[11,12,14,20] have recently been reported involving contact area reduction via crack-like ''detachment fronts''[12] preceding frictional motion. When the applied shear force F_S is not uniformly distributed along the interface, arrested (precursory) detachment fronts[20] are excited for F_S well below the threshold for macroscopic frictional motion at $F_S = \mu_S F_N$ (where μ_S is the static friction coefficient).

Upon cessation of motion, contacts re-form and strengthen. In many materials, interface strengthening is attributed to growth of A through contact rejuvenation[6,7,13] as frictional strength (embodied in μ_S) increases logarithmically with the time of static contact[8,9,21,22]. These slow changes, referred to as 'ageing', are common to a class of 'glassy' physical systems that are characterized by the existence of a large number of meta-stable configurations in which a system can dwell, while slowly relaxing to states of lower energy[15]. The way in which a frictional system evolves to this asymptotic logarithmic dependence, while regularizing the apparent singularity of μ_S at short times has been, until now, experimentally inaccessible. Here we examine how the local values of the real contact area $A(x, t)$ and concurrent slip $\delta(x, t)$ are related throughout detachment, slip and rehealing. These measurements provide an inclusive picture of processes that occur within frictional slip.

Our experimental system is schematically shown in Fig. 1a. Two poly(methyl methacrylate) (PMMA) blocks form a long (200 mm) and thin (6 mm) interface of approximately 1 μm root-mean-square roughness. The blocks are initially pressed together by a fixed, spatially uniform normal force F_N. F_S is applied to the upper block's 'trailing' edge at $x = 0$. $A(x, t)$ is measured[12,13] (see Supplementary Information) by illuminating the interface area with a laser sheet whose incident angle is well beyond the angle for total internal reflection from non-contacting parts of the interface. Under these conditions, the light intensity transmitted at each point x along the interface is proportional to $A(x, t)$. This light is imaged by a fast camera, capturing changes in $A(x, t)$ that occur over timescales ranging from 10^{-6} s to 10^{2} s (each of the camera's 1,280 pixels is mapped to a 0.2 mm × 0.8 mm region of the interface). In parallel to contact measurements, concurrent high-resolution displacement measurements are performed at specific points X adjacent to the interface.

When F_S is slowly increased, the spatially non-uniform shear stress distribution along the interface gives rise to a sequence (Fig. 1b) of arrested (precursory) detachment fronts[20]. Each successive front in the sequence initiates at the sample's trailing edge ($x = 0$), and propagates an increased distance before arresting within the interface. At every point along its path, each detachment front both generates a sharp reduction in $A(x, t)$ and initiates slip $\delta(x, t)$. No overall motion of the blocks occurs[20] until the fronts reach the leading edge ($x = L$). A close look (for example, Fig. 1c) reveals that detachment fronts are extremely rapid, with velocities that approach the Rayleigh-wave speed c_R (1,280 m s^{-1}). These high speeds suggest that the processes of detachment, slip and subsequent rehealing of the interface must initiate at extremely short (microsecond) timescales.

Arrested detachment fronts provide a sharp, well-defined initiation point for the study of the concurrent evolution of the surface area and slip. Acoustic signals initiated by each front were used both to trigger data storage and to suspend F_S for fixed periods (5–1,000 s) to study the resulting contact rejuvenation. In Fig. 2a we present simultaneous measurements of $A(t) \equiv A(X, t)$ and $\delta(t) \equiv \delta(X, t)$ at short timescales within the 500 μs that bracket the passage of a detachment front at point X. These measurements reveal three distinct dynamic phases:

[1]The Racah Institute of Physics, The Hebrew University of Jerusalem, Givat Ram, Jerusalem 91904, Israel. †Present address: School of Engineering and Applied Sciences, Harvard University, Cambridge, Massachusetts 02138, USA.

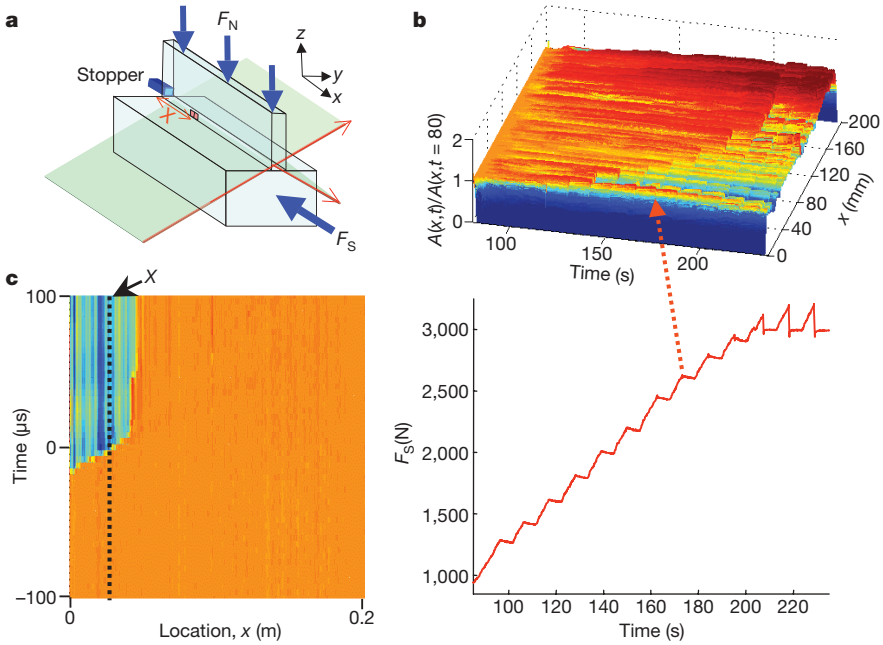

Figure 1 | Rapid precursors to frictional motion enable the precise study of local dynamics. a, Schematic diagram of the experimental system (see Supplementary Information). A uniform normal load F_N is applied to two PMMA blocks (base and top blocks). Shear force F_S is applied in the x direction to the base block, which is mounted on a low-friction stage. F_S is countered by a rigid stopper at the slider's $x = 0$ edge. The real area of contact $A(x, t)$ throughout the contact plane is imaged at 4-μs intervals. Simultaneous measurements of slip both at a distance X from the stopper and at the top block's leading edge were made. **b**, The non-spatially uniform shear loading generates a sequence of rapid precursors before the onset of overall motion, which initiate at $x = 0$ and arrest at successively larger distances within the interface. The top panel shows $A(x, t)$ normalized by $A(x, t = 80\,\text{s})$ taken before the first precursor. Hotter colours (reds) denote increased $A(x, t)$. Colder colours (blues) denote reduced $A(x, t)$. Each precursor significantly reduces $A(x, t)$ along its length. The bottom panel shows the corresponding loading curve $F_S(t)$. On acoustic detection of each precursor, the continuous increase of F_S in time is paused for 5–1,000-s intervals. Slip, generated by each precursor at $x = 0$, gives rise to small sharp drops in F_S that are detectable due to the compliance of the loading system. Here, $F_N = 6{,}000$ N and $\mu_S = 0.51$, and the origin of t was the time at which F_S was applied. **c**, Short-time measurements of $A(x, t)$ (at 4-μs intervals) reveal that each precursor is a detachment front propagating along the interface at velocities v approaching the Rayleigh-wave speed $c_R = 1{,}280\,\text{m s}^{-1}$. Here $v = 1{,}200 \pm 100\,\text{m s}^{-1}$. The dotted line denotes the location X where slip $\delta(t)$ was measured. Here, $A(x, t)$ was normalized by its value at 1 ms before the front's passage.

detachment (phase I), rapid slip (phase II) and slow slip (phase III). The entire net reduction of $A(t)$ occurs in phase I, immediately upon the passage of the detachment front (top panel of Fig. 2b). Simultaneous measurements of $\delta(t)$ reveal that during this 20% drop of $A(t)$, no net slip takes place at all. As shown in the lower panel of Fig. 2b, the drop in $A(t)$ is always preceded by strong fluctuations of $\delta(t)$ of duration approximately 10 μs.

Only upon conclusion of the detachment phase does net slip in the system initiate. In Fig. 2c we present a superposition of 16 different experiments in which $\delta(t)$, normalized by the total slip of each event δ_{tot} is plotted. The rough collapse of the data (where δ_{tot} varies between 4 μm and 20 μm) reveals generic dynamics. Two distinct slip phases exist; a rapid slip phase (phase II) that commences immediately after detachment, followed by a slow slip phase (phase III). A number of characteristic features are apparent in Fig. 2c. First, in both phases II and III, slip occurs at roughly constant slip velocities $\dot{\delta}$, the values of which differ by over an order of magnitude. Second, there is a characteristic duration time for each phase and the transition between them is sharp. The data collapse in Fig. 2c is due both to the existence of this characteristic time and to a roughly constant proportion of the total amount of slip within each phase. These features are independent of the magnitude of δ_{tot}, the measurement location X, the relative location between the front arrest point and X, details of loading and the geometry of the blocks (see Supplementary Information).

Phase II is characterized by its high slip velocities, ranging from $5\,\text{cm s}^{-1}$ to over $30\,\text{cm s}^{-1}$, with variations of $A(t)$ that are an order of magnitude smaller than those in phase I. The duration of this phase is a surprisingly constant 60 μs. This timescale is evident from both the transition point between phases II and III in Fig. 2c and the constant value (60 ± 6 μs) of the slope of the slip δ_{rapid} versus the slip velocity V_{rapid} in this phase, as presented in the top panel of Fig. 2d. We observe these features at all locations traversed by rapid ($0.8 < v/c_R < 1$) detachment fronts.

In phase III the slip is about 30% of δ_{tot}. $\dot{\delta}$ is much slower (in the range $0.1–2\,\text{cm s}^{-1}$) than in phase II, as shown in the bottom panel of Fig. 2d. The slip duration, however, is much longer (typically 350 μs). In this phase, $A(t)$ is constant in time with fluctuations of less than 1%.

Phase III concludes with the cessation of slip. This point marks the initiation of the contact rejuvenation and strengthening that are generally associated with 'ageing' of μ_S. Whereas the short-time (that is, less than a millisecond) evolution of μ_S is nearly impossible to measure directly, we can access the short-time evolution of frictional strength by measuring the growth of $A(t)$ from the time $t = t_0$, when slip ceases. At large times ageing is logarithmic. This growth must, however, be regularized at short times, because frictional strength is finite at the onset of growth. How this regularization occurs is unknown, because the short-time growth of neither μ_S nor $A(t)$ has ever been measured. Both the short- and long-time asymptotic behaviours can, in general, be characterized by the functional form: $A(t) = A(t_0) + b\log[f(t/\tau)]$, where $f(t = t_0) = 1$ and $f(t) \approx t^{\alpha}$ for $t \gg \tau$ (where α is any number), and τ is a characteristic timescale that renders t dimensionless. The simplest such function[21,23] is:

$$A(t) = A(t_0)[1 + \beta\log(1 + (t - t_0)/\tau)] \quad (1)$$

In Fig. 3a we describe the evolution of $A(t)$ over six orders of magnitude of temporal scales. In this region of growth, denoted phase IV, we observe logarithmic growth at long timescales. Figure 3a demonstrates that equation (1) provides an excellent characterization of $A(t)$ over the entire measurement range and shows

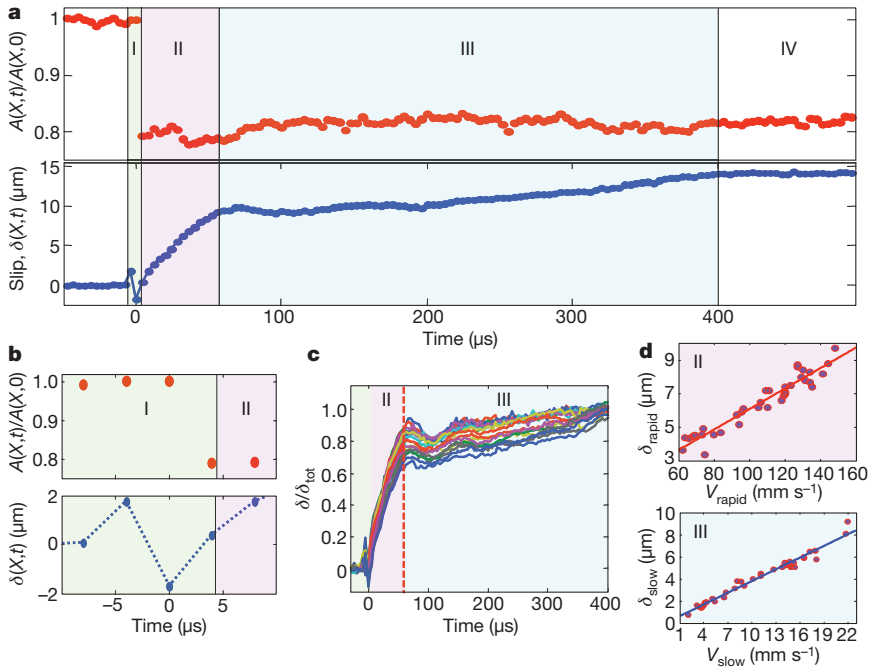

Figure 2 | The detachment process and the evolution of frictional slip. **a**, Simultaneous measurements of the local dynamics of contact area $A(t) \equiv A(X, t)$ (top panel) and slip $\delta(t) \equiv \delta(X, t)$ (bottom panel) before, during and after the passage of a precursor event. The measurements reveal three distinct initial phases of the dynamics: detachment (phase I) at $t = 0$, rapid slip (phase II) and slow slip (phase III). Notice that, whereas $A(t)$ drops by 20% in phase I, it remains nearly constant within phases II and III. **b**, The detachment phase (top panel), is labelled as phase I. No net slip (bottom panel) is observed before contact reduction. Nearly all reduction of $A(t)$ occurs within our 4-μs temporal resolution. The drop in $A(t)$ is concurrent with the conclusion of a short slip fluctuation. **c**, Normalizing $\delta(t)$ by the total slip in an event δ_{tot} yields an approximate collapse of the slip history. 16 events are plotted. Rapid slip (phase II), at roughly constant velocity V_{rapid}, initiates immediately upon the conclusion of the detachment phase. A sharp transition (denoted by the red dashed line) to velocities an order of magnitude lower V_{slow} is apparent (phase III). The approximate collapse indicates that both the relative part of the slip and the duration of each phase are approximately constant. **d**, The top panel shows the slope of the slip during rapid phase δ_{rapid} as a function of the slip velocity V_{rapid}, revealing the remarkably constant 60-μs duration of phase II. The bottom panel shows a similar plot of the slip δ_{slow} as a function of its corresponding velocity V_{slow}, yielding a typical duration of 350 μs for phase III. Solid lines depict linear fits to the data.

how $A(t)$ is regularized for short timescales. We note that the growth depicted in Fig. 3 does not simultaneously occur at every point along the interface, but initiates locally at each point upon cessation of slip.

Any deviation from equation (1) would be expected at times when $0 < (t - t_0)/\tau < 10$. In Fig. 3b, we plot $A(t)$ for a number of typical experiments in this range. Remarkably, the data all collapse and no systematic deviations from equation (1) are evident. The ageing rate β_S of the static friction coefficient, $\mu_S = \mu_S^0 + \beta_S \log(t)$, is given by[7] $\beta_S = \beta\mu_S$. The average value derived from our experiments of $\beta_S = 0.009 \pm 0.001$ is compatible with measurements in bulk frictional motion[21].

The timescale τ in equation (1) characterizes the growth rate of A, until $(t - t_0)/\tau \gg 1$. What determines this scale? In Fig. 3c we plot the value of τ as a function of the slip velocity, $\dot{\delta} = V_{slow}$, in phase III, which immediately preceded the onset of growth of $A(t)$ at t_0. We find that τ is inversely proportional to V_{slow}. A linear fit $\tau = D/V_{slow}$ (see Fig. 3c) yields $D = 0.9$ μm, a value corresponding to the characteristic size of the asperities in our experiments. We therefore interpret τ to be the effective contact time of the micro-contact population at the onset of ageing.

We now consider the overall evolution of the system, as described by phases I to IV. Two rough surfaces are 'bound' together by interlocking protrusions (asperities) from each surface. For any motion to occur, these asperities must circumvent one another, either by fracture, internal damage or deformation. Each process involves a significant energy cost that should scale with $A(x, t)$. Thus, the onset of slip involves a 'fracture energy' Γ, defined as the energy per unit area needed to detach two contact surfaces. In tensile fracture of PMMA, Γ is dominated by (irreversible) plastic deformation before bond rupture. We assume that similar plastic deformation of interlocking asperities is needed to enable motion.

In phase I the 'instantaneous' drop of $A(t)$ indicates that the contact fracture takes place within the short (about a microsecond) passage time of a detachment front. This drop is immediately preceded by strong fluctuations of $\delta(t)$ (see Fig. 2b), the magnitude of which approaches asperity sizes. We therefore surmise that this is when fracture occurs.

The heat ΓA released by this rapid irreversible deformation is deposited along the interface layer before the net slip. Such a rapid heat injection will cause an 'immediate' large temperature increase ΔT within the thin interface layer, akin to the large ($\Delta T \approx 1{,}000\,^{\circ}$C) temperature rises observed in the tensile fracture of PMMA[24]. Any increase beyond the glass temperature T_g (~110 °C in PMMA[10]) will cause significant shear strength weakening until the heat generated by fracture diffuses away from the interface region. An estimate of Γ (see Supplementary Information) yields cooling times compatible with the observed 60 μs duration of phase II.

An interface's overall strength is determined by both the value of A and the contacts' shear strength. A does not vary significantly between phases II and III, so the rapid slip in phase II clearly suggests contact strength weakening. Although conceptually similar to friction reduction attributed[25–27] to 'flash heating', fracture-generated weakening requires no sustained net slip to reduce shear strength. The thermally induced weakening here is sustained only for a finite time before cooling occurs. Although our interpretations of phases II and III are strictly relevant for glassy materials, it is interesting that the form of the slip profiles and the velocities measured in phases II and III resemble slip within granite blocks[18,19] during propagation of rapid crack-like fronts. This may suggest a similar fracture-induced weakening mechanism in brittle materials such as rock, where weakening via the crushing of interlocking asperities could supplant the thermal softening of PMMA.

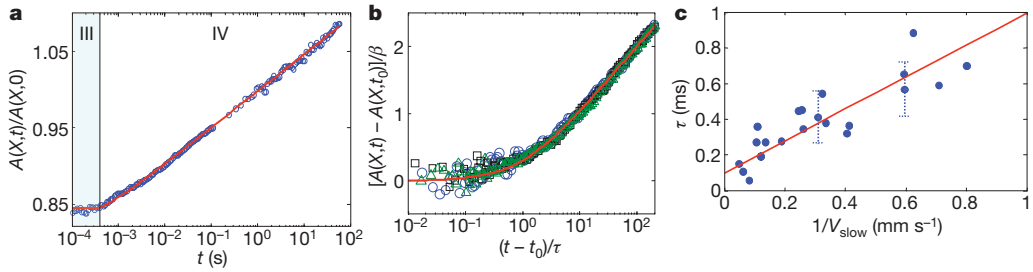

Figure 3 | Cessation of slip and interface ageing. **a**, $A(t)$ is plotted over six orders of magnitude of time, where $t = 0$ marks the drop in $A(t)$ within phase I. The transition from the constant value of $A(t)$ within phase III to purely logarithmic ageing is described by the red line, $A(t) = A(t_0)[1 + \beta\log(1 + (t - t_0)/\tau)]$, where t_0 is the time of slip arrest. **b**, A high-resolution plot of $[A(t) - A(t_0)]/\beta$ as a function of the scaled time $(t - t_0)/\tau$ for three typical experiments with $\tau = 310$ μs (squares), 450 μs (circles) and 470 μs (triangles). The excellent superposition indicates that all are described by the same functional form. The function $\log[1+(t - t_0)/\tau]$ (red line) describes the data with no visible systematic deviations. **c**, The characteristic timescale τ as a function of $1/V_{slow}$. The data suggest a linear dependence of $\tau = D/V_{slow}$, where a fit yields a length scale $D \approx 0.9$ μm, consistent with the characteristic scale of the asperities in our experiments. Thus, τ represents the characteristic timescale of the system's memory and may be interpreted as the effective asperity contact time during phase III. Error bars represent the cumulative error in each measurement (for details, see Supplementary Information).

In glasses, when the softened layer cools to below T_g, contact strengthening will occur and the system will undergo a sharp transition to slow slip, precisely as observed in phase III. The local motion in this phase may be analogous to large-scale frictional motion[8,9] governed by the contact dynamics of 'rigid' (unsoftened) micro-contacts. Here, 'collective' heating due to fracture is absent, because slip is accomplished by sporadic rupture of discrete, loosely coupled contacts. The interface resembles a glassy system in which the state of each contact is coupled only to that of its neighbours through the residual shear stress that remained at the transition from phase II.

In phase IV equation (1) both shows how logarithmic ageing is regularized and relates the early time growth rate τ to the slip history immediately before slip cessation. Precisely this behaviour was suggested[16] in recent interpretations of experiments describing granite blocks sliding over a ground quartz (gouge) layer[22]. V_{slow} is an ensemble average over numerous micro-contacts, so τ reflects the collective behaviour or 'state' of the entire ensemble. In our measurements, V_{slow} and thus τ are spatially local, and suggest that the system's state is a local 'coarse-grained' quantity that represents an ensemble average of the contact population at each spatial location. It is significant that τ is determined by the slip rate in phase III. Thus, the overall dynamics of ageing retains a memory of the system's state at the arrest of slip.

These results provide fundamental new insights into how frictional strength evolves throughout the slip–stick cycle. They suggest that a mesoscopic description of friction that incorporates the spatial dependence of the system's state may be necessary when describing dynamics at either the intermediate timescales within phases III and IV, or in large spatially extended systems.

Received 27 August; accepted 10 November 2009.

1. Scholz, C. H. Earthquakes and friction laws. *Nature* **391,** 37–42 (1998).
2. Dieterich, J. H. Earthquake nucleation on faults with rate-dependent and state-dependent strength. *Tectonophysics* **211,** 115–134 (1992).
3. Marone, C. Laboratory-derived friction laws and their application to seismic faulting. *Annu. Rev. Earth Planet. Sci.* **26,** 643–696 (1998).
4. Ben-Zion, Y. Collective behavior of earthquakes and faults: continuum-discrete transitions, progressive evolutionary changes, and different dynamic regimes. *Rev. Geophys.* **46,** 1–70 (2008).
5. Urbakh, M., Klafter, J., Gourdon, D. & Israelachvili, J. The nonlinear nature of friction. *Nature* **430,** 525–528 (2004).
6. Dieterich, J. H. & Kilgore, B. D. Direct observation of frictional contacts—new insights for state-dependent properties. *Pure Appl. Geophys.* **143,** 283–302 (1994).
7. Bowden, F. P. & Tabor, D. *The Friction and Lubrication of Solids* Ch. 1 (Oxford Univ. Press, 2001).
8. Dieterich, J. H. Modeling of rock friction. 1. Experimental results and constitutive equations. *J. Geophys. Res.* **84,** 2161–2168 (1979).
9. Rice, J. R. & Ruina, A. L. Stability of steady frictional slipping. *J. Appl. Mech.* **50,** 343–349 (1983).
10. Baumberger, T., Berthoud, P. & Caroli, C. Physical analysis of the state- and rate-dependent friction law. II. Dynamic friction. *Phys. Rev. B* **60,** 3928–3939 (1999).
11. Ben-Zion, Y. Dynamic ruptures in recent models of earthquake faults. *J. Mech. Phys. Solids* **49,** 2209–2244 (2001).
12. Rubinstein, S. M., Cohen, G. & Fineberg, J. Detachment fronts and the onset of dynamic friction. *Nature* **430,** 1005–1009 (2004).
13. Rubinstein, S., Cohen, G. & Fineberg, J. Contact area measurements reveal loading-history dependence of static friction. *Phys. Rev. Lett.* **96,** 256103 (2006).
14. Xia, K., Rosakis, A. J. & Kanamori, H. Laboratory earthquakes: the sub-Raleigh-to-supershear rupture transition. *Science* **303,** 1859–1861 (2004).
15. Rottler, J. & Robbins, M. O. Unified description of aging and rate effects in yield of glassy solids. *Phys. Rev. Lett.* **95,** 225504 (2005).
16. Nakatani, M. & Scholz, C. H. Intrinsic and apparent short-time limits for fault healing: theory, observations, and implications for velocity-dependent frictionl. *J. Geophys. Res. Solid Earth* **111,** B12208 (2006).
17. Kim, H. J., Kim, W. K., Falk, M. L. & Rigney, D. A. MD simulations of microstructure evolution during high-velocity sliding between crystalline materials. *Tribol. Lett.* **28,** 299–306 (2007).
18. Ohnaka, M. & Kuwahara, Y. Characteristic features of local breakdown near a crack-tip in the transition zone from nucleation to unstable rupture during stick-slip shear failure. *Tectonophysics* **175,** 197–220 (1990).
19. Okubo, P. G. & Dieterich, J. H. Effects of physical fault properties on frictional instabilities produced on simulated faults. *J. Geophys. Res.* **89,** 5817–5827 (1984).
20. Rubinstein, S. M., Cohen, G. & Fineberg, J. Dynamics of precursors to frictional sliding. *Phys. Rev. Lett.* **98,** 226103 (2007).
21. Berthoud, P. & Baumberger, T. G'Sell, C. & Hiver, J. M. Physical analysis of the state- and rate-dependent friction law: static friction. *Phys. Rev. B* **59,** 14313–14327 (1999).
22. Marone, C. The effect of loading rate on static friction and the rate of fault healing during the earthquake cycle. *Nature* **391,** 69–72 (1998).
23. Dieterich, J. H. Time-dependent friction in rocks. *J. Geophys. Res.* **77,** 3690–3697 (1972).
24. Fuller, K. N. G., Fox, P. G. & Field, J. E. Temperature rise at tip of fast-moving cracks in glassy polymers. *Proc. R. Soc. Lond. A* **341,** 537 (1975).
25. Rice, J. R. Heating and weakening of faults during earthquake slip. *J. Geophys. Res. Solid Earth* **111,** B05311 (2006).
26. Nielsen, S., Di Toro, G., Hirose, T. & Shimamoto, T. Frictional melt and seismic slip. *J. Geophys. Res. Solid Earth* **113,** B01308 (2008).
27. Beeler, N. M., Tullis, T. E. & Goldsby, D. L. Constitutive relationships and physical basis of fault strength due to flash heating. *J. Geophys. Res. Solid Earth* **113,** B01401 (2008).

Supplementary Information is linked to the online version of the paper at www.nature.com/nature.

Acknowledgements We acknowledge comments by J. R. Rice, M. O. Robbins, T. Baumberger and C. Caroli. This work, as part of the ESF EUROCORES programme FANAS, was supported by the Israel Science Foundation (grant 57/07). We also acknowledge support of the US–Israel Binational Science Foundation (grant 2006288).

Author Contributions All authors contributed to the design of the experiment. O.B.-D. performed the measurements. All authors contributed to the analysis and writing of the manuscript.

Author Information Reprints and permissions information is available at www.nature.com/reprints. The authors declare no competing financial interests. Correspondence and requests for materials should be addressed to J.F. (jay@vms.huji.ac.il).